

© © 2014 IEEE. Personal use of this material is permitted. Permission from IEEE must be obtained for all other uses, in any current or future media, including reprinting/republishing this material for advertising or promotional purposes, creating new collective works, for resale or redistribution to servers or lists, or reuse of any copyrighted component of this work in other works.

Title: Concurrent Self-Organizing Maps for Supervised/Unsupervised Change Detection in Remote Sensing Images

This paper appears in: IEEE Journal of Selected Topics in Applied Earth Observations and Remote Sensing

Date of Publication: 22 July 2014

Author(s): Victor Neagoe, Radu Stoica, Alexandru Ciurea, Lorenzo Bruzzone, Francesca Bovolo

Volume: 7, Issue: 8

Page(s): 3525 - 3533

Product Type: Journals & Magazines

DOI: 10.1109/JSTARS.2014.2330808

URL: <http://dx.doi.org/10.1109/JSTARS.2014.2330808>

Concurrent Self-Organizing Maps for Supervised/Unsupervised Change Detection in Remote Sensing Images

Victor Neagoe, *Senior Member, IEEE*, Radu Stoica, Alexandru Ciurea,
Lorenzo Bruzzone, *Fellow, IEEE*, Francesca Bovolo, *Senior Member, IEEE*

Abstract—This paper proposes two approaches to change detection in bi-temporal remote sensing images based on Concurrent Self-Organizing Maps (CSOM) neural classifier. The first one performs change detection in a supervised way, whereas the second performs change detection in an unsupervised way. The supervised approach is based on two steps: (i) Concatenation (CON); and (ii) CSOM classification. CSOM classifier uses two SOM modules one associated to the class of change and the other to the class of no-change for the generation of the training set. The unsupervised change detection approach is based on 4 steps: (i) image comparison (IC), consisting in either computation of difference image (DI) for passive sensors or computation of log-ratio image (LRI) for active sensors; (ii) unsupervised selection of the pseudo-training sample set (USPS); (iii) concatenation (CON); and (iv) CSOM classification. The proposed approaches are evaluated using two datasets. First dataset is a LANDSAT-5 TM bi-temporal image over Mexico area taken before and after two wildfires; the second one is a TerraSAR-X image acquired in the Fukushima region, Japan, before and after tsunami. Experimental results confirm the effectiveness of the proposed approaches.

Index Terms—Supervised/unsupervised change detection, multitemporal images, Concurrent Self-Organizing Maps (CSOM), remote sensing images

I. INTRODUCTION

Change detection aims to identify land-cover changes between two co-registered remote sensing images acquired over the same geographical area at two different time instants [1]. In the literature, automatic change detection in digital images has become an increasingly important topic in the field of satellite image processing. Its applications plays a relevant role in environmental studies, which requires knowledge about the evolution of slow phenomena and/or rapid abrupt changes. Examples of such phenomena are crop monitoring, land-cover shift analysis, deforestation

monitoring, urban growth, flood and fire control [2], [3], [4], [5], [6]. The relevance of such kind of analysis is confirmed by some activities carried out at European level such as the database of land changes between 2000-2006, based on standard CORINE land cover categories [7], [8] compiled by the European Environmental Agency (EEA).

In this manuscript the focus is on damage assessment related to natural disasters application, such as changes caused by earthquakes [9], tsunamis [10], fires [11], etc. In the last decades, the frequency of such events has increased dramatically [12] therefore there is a rising interest in the scientific community for defining methods that can help in mitigating their effects and performing an automatic and fast assessment of the extension of the damages.

Numerous algorithms have been proposed for the automatic detection of changes [10], [13], [3], [14], [15], [16], [17]. These algorithms can be grouped in two large classes: *supervised* and *unsupervised* techniques. The supervised methods require a multitemporal ground truth information, but usually achieve higher performance. However the ground truth information collection requires a significant effort from the economical and practical view point [18]. The unsupervised approaches perform a direct comparison of the two multitemporal images and do not require any prior information about land-cover classes. Some examples of unsupervised methods can be found in [18], [1], [16]. The most common approach to unsupervised change detection is based on thresholding of the image obtained after comparison. However more unsupervised complex approaches exist. As an example in [13] an unsupervised approach is proposed which is based on Support Vector Machine (SVM). Here a pseudo-training set for SVM learning phase is generated in an unsupervised way by taking advantage of the a priori knowledge on the behavior of change and no-change class in the difference image.

Among the change detection approaches, in the last years there have been proposed several techniques based on Artificial Neural Networks (ANN) [15], [19], [20], which have been previously successfully applied for image analysis and segmentation tasks. ANN presents several advantages over other classification methods [6], such as: (i) automatic adjustment to the classified data, without requiring any a priori models; (ii) they can be used as universal function approximators; (iii) they can be applied to non-linear and

Manuscript received on October 15, 2013.

V.-E. Neagoe, R.-M. Stoica, and A.-I. Ciurea are with the Department of Applied Electronics and Information Engineering, “Politehnica” University of Bucharest, Bucharest, Romania (email: victor.neagoe@upb.ro)

L. Bruzzone is with the Department of Information Engineering and Computer Science, University of Trento, Trento, Italy (email: lorenzo.bruzzone@ing.unitn.it)

F. Bovolo is with the Center for Information and Communication Technology, Fondazione Bruno Kessler, Trento, Italy (email: bovolo@fbk.eu)

discontinuous data. Among neural networks we recall here the interesting example of Self-Organizing Map (SOM) (also called Kohonen network) as they have the peculiarity of being unsupervised. Neurons in them become specifically tuned to classes of patterns through a competitive, unsupervised or self-organizing learning [21].

Starting from the idea to consider the SOM as a cell characterizing a specific class, Neagoe et al [22] proposed a new neural supervised classification model called Concurrent Self-Organizing Maps (CSOM). CSOM represents a collection of small SOM modules, which use a global winner-takes-all strategy. The mechanism is equivalent to generate by neural means an improved training set and to use this virtual training set as reference for a Nearest Neighbor (NN) classifier. In [23] CSOM model has been applied for static multispectral image classification. Here we expand the use of to the detection of land-cover changes in time-series of remote sensing images in the context of both a supervised and an unsupervised change detection. The supervised approach consists of two steps: (i) concatenation of multitemporal image features; and (ii) classification by CSOM. The unsupervised approach is based on four steps: (i) image comparison; (ii) unsupervised generation of the pseudo-training set; (iii) concatenation of multitemporal image features; and (iv) classification by CSOM.

II. PROPOSED SUPERVISED CHANGE DETECTION APPROACH BASED ON CSOM

The proposed supervised change detection approach is based on: (i) concatenation of multitemporal image features (CON); and (ii) Concurrent Self-Organizing Maps (CSOM) classification (Fig. 1). We will refer to it as Concatenation-based Concurrent Self-Organizing Maps (C^2 SOM).

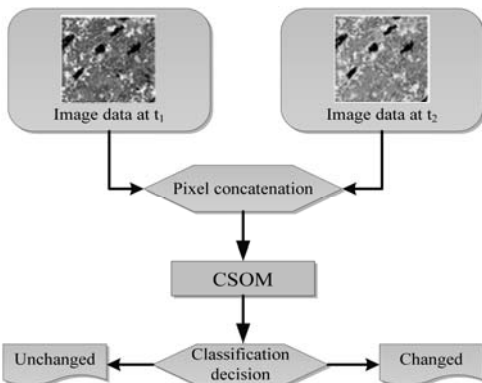


Fig. 1. Block scheme of the proposed supervised change detection approach.

A. Concatenation

Feature concatenation is used to build the feature vector to be given as input to the CSOM classifier [20]. Let $A^T = [a_1 \dots a_n]^T$ and $B^T = [b_1 \dots b_n]^T$ be the n -dimensional feature vectors characterizing each spatial position in the images acquired at time t_1 and t_2 , respectively. After concatenation, each spatial position will be modeled by a $2n$ -dimensional feature vector V^T defined as

$$V^T = [A^T B^T] = [a_1 \dots a_n b_1 \dots b_n]^T. \quad (1)$$

B. CSOM Classification

The classification step is performed by the Concurrent Self-Organizing Maps (CSOM) neural classifier [22], [23] extended to the use in the multitemporal domain. To this end Concurrent Self-Organizing Maps (CSOMs) combines SOM modules in a new complex network, which uses a winner-takes-all strategy for assigning the output class [22]. The number of SOM modules equals the number of classes (for change detection, one has two classes). Each SOM is trained in an unsupervised manner to correctly classify the patterns of one class only (i.e., change or no-change). Thus each SOM is trained with the subset of samples having the same class label as SOM label (Fig. 2). The global training algorithm is supervised, but each SOM uses an unsupervised training technique.

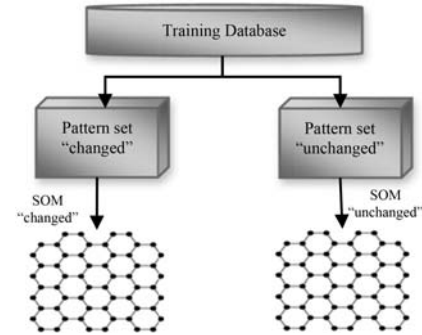


Fig. 2. The CSOM training model.

The CSOM technique is equivalent to substitute the real training samples by SOM generated virtual samples and then to apply the nearest neighbor (NN) classifier using as reference all the pseudo-training samples. After CSOM training, each $2n$ -dimensional input vector is assigned to the change or no-change class according to the label of the nearest CSOM neuron by minimizing the Euclidean distance.

III. PROPOSED UNSUPERVISED CHANGE DETECTION APPROACH BASED ON CSOM

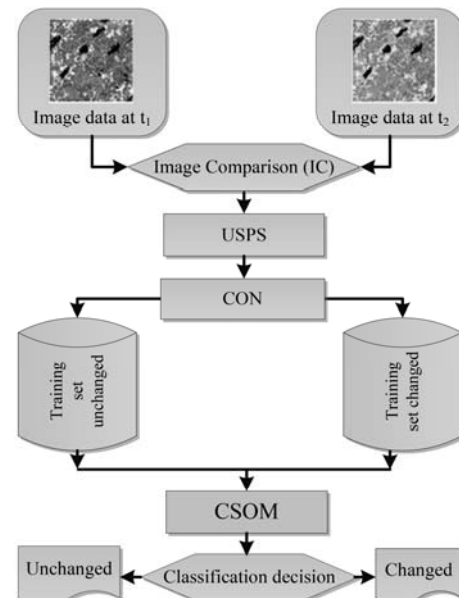


Fig. 3. Block scheme of the proposed unsupervised change detection approach.

The proposed unsupervised change detection approach is based on four steps: (i) image comparison (IC); (ii) unsupervised generation of the pseudo-training set (USPS); (iii) concatenation of multitemporal image features (CON); and (iv) classification by CSOM (Fig. 3).

A. Multitemporal image comparison (IC)

Let us consider a generic pixel of the two considered n -dimensional images. Comparison is performed in different ways according to whether the multitemporal images are acquired by active or passive sensors.

In the case of multispectral images acquired by passive sensors comparison can be performed by computing the magnitude of the Spectral Change Vectors (SCV) obtained by standard Change Vector Analysis (CVA) approach as [18].

$$d = \sqrt{\sum_{i=1}^n (b_i - a_i)^2} \quad (2)$$

where d is the SCV magnitude image. In such image changed samples assume large values, whereas unchanged samples assumes small values.

In the case of images acquired by active sensors like Synthetic Aperture Radar (SAR) images comparison is commonly performed by applying the log-ratio operator [11]. Sample feature vectors are 1-dimensional ($n = 1$) and the log-ratio image (lr) is defined as

$$lr = \log \frac{b_1}{a_1} = \log b_1 - \log a_1 \quad (3)$$

In lr unchanged pixels assumes values around zero and changed pixels assume values far from zero.

B. Unsupervised Selection of the Pseudo-Training Set (USPS)

The behaviors of change and no change classes are exploited in this step to define a pseudo-training set in an unsupervised way to be used as input for the next step of classification. The approach is based on unsupervised threshold selection [13], [1]. A threshold T is first computed that separates changed from unchanged pixel [1] according to the Bayes decision. The desired set of pixels with a high probability to be assigned to the class of change or no-change is obtained by defining an uncertainty region around T that identifies highly uncertain pixels [13]. This region includes samples having magnitude in $[T-\delta_1, T+\delta_2]$. Samples showing magnitude larger than $T+\delta_2$ have a high probability to be changed, whereas samples having magnitude smaller than $T-\delta_1$ have a high probability to be unchanged. T is automatically estimated from the statistical distribution $p(d)$ of the magnitude image. A similar mechanism can be adopted for the analysis of lr . Fig. 4 gives an overview of the mechanism.

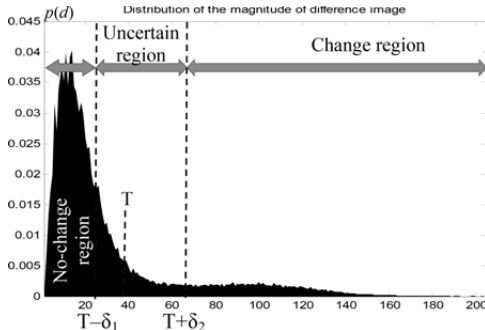


Fig. 4. Distribution $p(d)$ of the samples in the SCV magnitude image d and relevant decision regions for pseudo-training set definition.

C. Concatenation and CSOM Classification (C^2SOM)

The third and fourth steps are the same as the ones in Sec. II.A. The unsupervised change detection is carried out by using the Concurrent Self-Organizing Maps (CSOM) neural classifier [15], [22], [23], applied to concatenated vectors.

IV. EXPERIMENTS AND RESULTS

A. Experimental set-up

The two approaches to change detection have been tested on three multitemporal datasets. In order to demonstrate its effectiveness results achieved with the proposed methods have been compared with ones obtained with: Bayes and Nearest Neighbor statistical classifiers; MLP neural classifiers; and SVM with radial-basis function (RBF) kernel.

The Bayes (likelihood) classifier [1] performs decision according to

$$(X - \mu_c)^T \times \Sigma_c^{-1} \times (X - \mu_c) - (X - \mu_n)^T \times \Sigma_n^{-1} \times (X - \mu_n) + \ln \frac{\det \Sigma_c}{\det \Sigma_n} < 2 \ln \frac{P(\omega_c)}{P(\omega_n)} \quad (4)$$

where class conditional probability density functions have been implicitly considered as being Gaussian distributed. μ_c , μ_n , Σ_c , Σ_n , $P(\omega_c)$ and $P(\omega_n)$ are the average vectors, the covariance matrices and the prior probabilities of change and no-change classes, respectively. All the above parameters are computed in a supervised way from the training set.

The Nearest Neighbor (NN) classifier assigns the class by computing the distance from the input vector to each of the training vectors and by selecting the label of the nearest neighbor.

MLP classifier is the standard neural network for pattern recognition tasks [24]. For change detection, an MLP configuration has been considered with $2n$ input neurons (one for each of the features in the concatenated vector) and 2 output neurons (one for change class and one for no-change class). Here an architecture with one hidden layer has been considered and the number of neurons in the hidden layer varied between 5 and 25. The learning rate was set to 0.01 and momentum constant to 0.9.

The Radial Basis Function (RBF) neural network has a three layer architecture similar to that of MLP [24]. Here a Gaussian activation function for the hidden layer neurons has been considered. The RBF kernel spread parameter has been varied between 1 and 1000. Due to the nonlinearity of its hidden layer activation function, an RBF network can better approximate a desired pattern by comparison to MLP.

Support Vector Machine (SVM) is a supervised machine learning classifier based on a nonlinear mapping of the input vectors to a higher dimensional space [24]. The mapping is done based on a selected kernel function. For the present experiments, we have chosen a kernel based on radial basis functions (RBF), namely a Gaussian function. Model selection has been performed according to a grid search strategy varying the spread between 0.001 and 100.

For the CSOM classifier, two neighborhood map lattices were considered: rectangular and hexagonal, combined with three different architectures: sheet, cylindrical and toroidal. The size range of SOM modules are from 2×2 till 25×25 neurons.

Change detection performance for the proposed methods

and the reference one has been evaluated according to standard indexes. In greater detail missed alarms, false alarms and total errors have been computed in terms of number of pixels. In addition, the overall accuracy (OA), missing alarm rate (MAR), false alarm rate (FAR) in percentage have been given for each trial. Finally, the kappa accuracy is provided.

B. Mexico data set

B1) Dataset description

We have firstly experimented the proposed change detection techniques on the selection of 2 bands (namely 4 and 5) acquired by the Thematic Mapper (TM) sensor of the Landsat-5 satellite. The two images (512x360 pixels with 30 meters resolution) were acquired in April 2000 and May 2002 (Figs. 5(a) and (b)) over a Mexico area [13]. Between the two acquisition dates a forest fire destroyed a large part of the forest. Reference map has been built by experts according to both in filed campaigns and accurate photointerpretation refinement. The burned area (29506 pixels) represents the changed area in our dataset (coded with black color in Fig. 5 (b)). The remaining 154814 pixels represent the unchanged area.

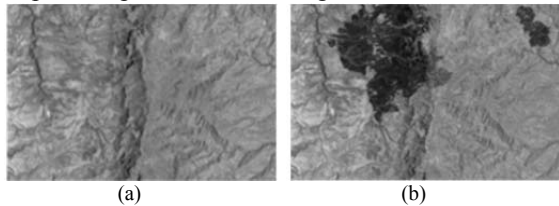


Fig. 5. Band 4 of the Landsat-5 TM image on the Mexico area. (a) April 2000. (b) May 2002.

B2) Results of the C²SOM Supervised Change Detection Model for Mexico Dataset

We have used a selection of 2000 pixels for the training set, out of which 1000 are labeled as changed and 1000 as unchanged. These represent 1.09% of the total pixels. The remained 182320 pixels (98.91%) are used for testing.

The first set of experiments aimed to compare CSOM classifier and reference classifiers taking into consideration their results in the best OA and MAR for the considered data set. Also, the optimization of the CSOM architecture and size has been performed at this stage. Tables I-IV show the results.

TABLE I
BEST OVERALL ACCURACY (OA) AS A FUNCTION OF CLASSIFIER TYPE (SUPERVISED APPROACH-MEXICO DATASET).

Classifier	Parameters	False alarms		Missed alarms		Overall error	OA (%)	Kappa Accuracy
		# pixels	%	# pixels	%			
1-NN	-	6095	3.96	1238	4.34	7333	95.98	0.857
Bayes	-	10829	7.04	1730	6.07	12559	93.11	0.769
MLP	1 hidden layer 12 neurons	3876	2.52	1300	4.56	5176	97.16	0.896
RBF	Spread=31	3593	2.35	1518	5.14	5111	97.20	0.897
SVM-RBF	Spread= 5	3914	2.54	1274	4.47	5188	97.15	0.896
CSOM	Hex sheet 20x8/16x3	2640	1.72	1505	5.28	4145	97.73	0.915

TABLE II
BEST MISS ALARM RATE (MAR) AS A FUNCTION OF CLASSIFIER TYPE (SUPERVISED APPROACH-MEXICO DATASET).

Classifier	Parameters	False alarms		Missed alarms		Overall error	OA (%)	Kappa accuracy
		# pixels	%	# pixels	%			
1-NN	-	6095	3.96	1238	4.34	7333	95.98	0.857
Bayes	-	10829	7.04	1730	6.07	12559	93.11	0.769
MLP	1 hidden layer 5 neurons	4753	3.09	641	2.25	5394	97.04	0.894
RBF	Spread=10	5245	3.41	1457	5.11	6702	96.33	0.868
SVM-RBF	Spread= 5	3914	2.54	1274	4.47	5188	97.15	0.896
CSOM	Rect Toroid 12x20/16x25	7807	5.08	467	1.64	8274	95.46	0.844

TABLE III
BEST OVERALL ACCURACY (OA) AS A FUNCTION OF CSOM ARCHITECTURE (MAR<25%) (SUPERVISED APPROACH-MEXICO DATASET).

Topology	SOM1/SOM2	False alarms		Missed alarms		Overall error	OA (%)	Kappa accuracy
		# pixels	%	# pixels	%			
Rect Toroid	6x20/3x15	3449	2.24	1168	4.1	4617	97.47	0.907
Rect Sheet	12x5/7x3	2693	1.75	1686	5.91	4379	97.6	0.910
Rect Cylinder	11x8/12x3	2597	1.69	1675	5.88	4272	97.66	0.912
Hex Toroid	8x17/3x12	2920	1.9	1399	4.91	4319	97.63	0.912
Hex Sheet	20x8/16x3	2640	1.72	1505	5.28	4145	97.73	0.915
Hex Cylinder	16x5/13x3	2853	1.85	1513	5.31	4366	97.61	0.911

TABLE IV
BEST MISS ALARM RATE (MAR) AS A FUNCTION OF CSOM ARCHITECTURE (OA>80%) (SUPERVISED APPROACH-MEXICO DATASET).

Topology	SOM1/SOM2	False alarms		Missed alarms		Overall error	OA (%)	Kappa Accuracy
		# pixels	%	# pixels	%			
Rect Toroid	12x20/16x25	7807	5.08	467	1.64	8274	95.46	0.844
Rect Sheet	7x18/11x23	7582	4.93	543	1.9	8125	95.54	0.847
Rect Cylinder	6x20/13x25	7290	4.74	484	1.7	7774	95.74	0.853
Hex Toroid	19x17/24x22	7179	4.67	514	1.8	7693	95.78	0.854
Hex Sheet	18x20/21x25	5862	3.81	628	2.2	6490	96.44	0.874
Hex Cylinder	7x20/10x25	6703	4.36	508	1.78	7211	96.04	0.862

The best results have been obtained by the proposed CSOM classifier, with a 97.73% Overall Accuracy and 1.64 % Miss Alarm Rate. The optimum CSOM architecture has proved to be the hexagonal sheet with modules of 20x8/16x3, maximizing both OA and Kappa. The best (minimum) MAR is obtained using a rectangular toroid with module sizes of 12x20/16x25.

The best benchmark classifiers reach OA less than the CSOM performance (97.73%), namely, between 97.15% for SVM, 97.16% for MLP and 97.20% for RBF. For the MAR, the advantage of CSOM over the benchmark classifiers is more significant, the nearest neighbor of CSOM being MLP with 2.25% (by comparison to 1.64% for CSOM).

We have also considered the evolution of the OA and MAR scores for various SOM module sizes, to deduce a potential correlation. Figs. 6 and 7 display the evolution of the two performance indicators for square SOM modules, in the size range from 5x5 to 20x20 neurons. By increasing the SOM size, one obtains a better OA and a better MAR.

One can remark that CSOM leads also to the best kappa accuracy of 0.915.

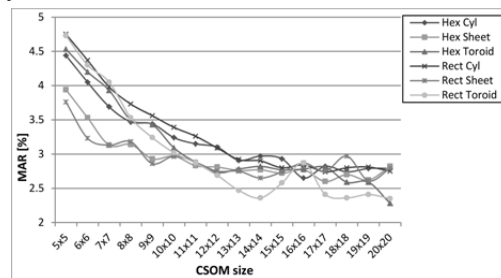


Fig. 6. Miss Alarm Rate (MAR) for different CSOM architectures as a function of SOM module size (Supervised approach-Mexico dataset) (lower is better)

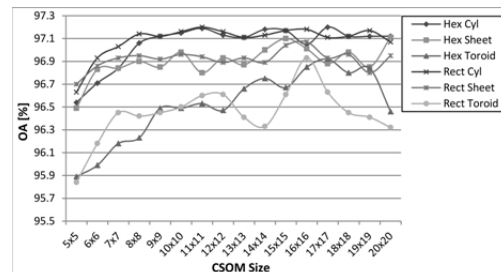


Fig. 7. Overall accuracy (OA) for different CSOM architectures (Supervised approach-Mexico dataset)

Fig. 8 shows as an example the change detection map obtained by using the CSOM classifier that resulted in the best overall accuracy.



Fig. 8. (a) Change detection map obtained by the supervised approach for Mexico dataset using CSOM (hexagonal sheet with module sizes 20x8/16x3). (b) Reference map (black pixels are changed; white pixels are unchanged).

B3) Results of the IC-USPS –C²SOM Unsupervised Change Detection Model for Mexico Dataset

The unsupervised selection of the pseudo-training set (USPS) selected 19798 changed pixels, 106484 unchanged pixels, and 58038 unlabeled pixels. The selected changed and unchanged pixels represent the pseudo-training set. The test set contains all the image pixels, labeled according to the truth reference map.

The experimental results of the proposed unsupervised approach for change detection are given in Tables V-VIII. The change map obtained by the best classifier (CSOM with symmetrical rectangular cylinder modules of 12 x 12) is shown in Fig. 9.

TABLE V
BEST OVERALL ACCURACY (OA) AS A FUNCTION OF CLASSIFIER TYPE (UNSUPERVISED APPROACH-MEXICO DATASET)

Classifier	Parameters	False alarms		Missed alarms		Overall error	OA (%)	Kappa accuracy
		# pixels	%	# pixels	%			
1-NN	-	3074	1.98	3840	13.01	6914	96.24	0.859
Bayes	-	3716	2.40	1489	5.04	5205	97.18	0.898
MLP	1 hidden layer 8 neurons	2064	1.33	3117	10.56	5181	97.18	0.893
RBF	Spread = 150	1972	1.27	2279	7.72	4251	97.69	0.913
SVM-RBF	Spread = 0.01	1128	0.72	3811	12.91	4939	97.32	0.896
CSOM	Rect cyl 11x19/11x19	2042	1.31	2042	6.92	4084	97.78	0.917

TABLE VI
BEST MISSED ALARM RATE (MAR) AS A FUNCTION OF CLASSIFIER TYPE (UNSUPERVISED APPROACH-MEXICO DATASET)

Classifier	Parameters	False alarms		Missed alarms		Overall error	OA (%)	Kappa accuracy
		# pixels	%	# pixels	%			
1-NN	-	3074	1.98	3840	13.01	6914	96.24	0.859
Bayes	-	3716	2.40	1489	5.04	5205	97.18	0.898
MLP	1 hidden layer 6 neurons	4981	3.21	1790	6.06	6771	96.32	0.869
RBF	Spread = 150	1972	1.27	2279	7.72	4251	97.69	0.913
SVM-RBF	Spread = 0.05	1272	0.82	3803	12.88	5075	97.24	0.893
CSOM	Rect toroid 25x25/25x25	4965	3.20	1131	3.83	6096	96.69	0.883

TABLE VII
BEST OVERALL ACCURACY (OA) AS A FUNCTION OF CSOM TOPOLOGY (MAR<25%) (UNSUPERVISED APPROACH-MEXICO DATASET)

Topology	Symmetrical SOM module size	False alarms		Missed alarms		Overall error	OA (%)	Kappa accuracy
		# pixels	%	# pixels	%			
Rect. Sheet	11x21	2328	1.50	1798	6.09	4126	97.76	0.917
Hexa. Sheet	11x19	2433	1.57	1713	5.80	4146	97.75	0.917
Rect. Cylindrical	11x19	2042	1.31	2042	6.92	4084	97.78	0.917
Hexa. Cylindrical	13x25	2288	1.47	1853	6.28	4141	97.75	0.916
Rect. Toroidal	15x24	3399	2.19	1468	4.97	4867	97.35	0.904
Hexa. Toroidal	17x21	3312	2.13	1489	5.04	4801	97.39	0.905

TABLE VIII
BEST MISSED ALARM RATE (MAR) AS A FUNCTION OF CSOM TOPOLOGY (OA>80%) (UNSUPERVISED APPROACH-MEXICO DATASET)

Topology	Symmetrical SOM module size	False alarms		Missed alarms		Overall error	OA (%)	Kappa accuracy
		# pixels	%	# pixels	%			
Rect. Sheet	11x25	2624	1.69	1631	5.52	4255	97.69	0.915
Hexa. Sheet	11x21	2459	1.58	1699	5.75	4158	97.74	0.916
Rect. Cylindrical	11x25	2286	1.47	1863	6.31	4149	97.74	0.916
Hexa. Cylindrical	11x25	2673	1.72	1681	5.69	4354	97.63	0.913
Rect. Toroidal	25x25	4965	3.20	1131	3.83	6096	96.69	0.883
Hexa. Toroidal	11x25	4106	2.65	1323	4.48	5429	97.05	0.894



Fig. 9. (a) Change detection map obtained by the unsupervised approach for Mexico dataset using CSOM (rectangular-cylindrical modules of sizes 12x12/12x12). (b) Reference map (black pixels are changed; white pixels are unchanged).

From Tables V and VI one can deduce that CSOM leads to best performances by comparison to the considered benchmark classifiers. The best overall accuracy result of 97.78% and the best Kappa accuracy of 0.917 have been obtained for a CSOM classifier (Table V). The best missed alarm rate of 3.83% (Table VI) corresponds also to CSOM classifier. Tables VII and VIII give the best performances (OA and respectively MAR) as a functions of CSOM module architecture and neighborhood lattice. The best OA is obtained using a CSOM architecture corresponding to a rectangular-cylindrical topology with symmetrical modules of sizes 11x19. The best (minimum) MAR is obtained using a rectangular lattice and toroidal architecture with symmetrical modules of sizes 25x25.

C. Fukushima dataset

C1) Fukushima dataset description

The second data set is composed of two 400 x 400 pixel radar brightness images (StripMap imaging mode, up to 3 meters resolution) acquired by TSX-1 sensor of TerraSAR-X Earth Observation satellite over the Fukushima region in Japan (Figs. 10(a) and (b)). The first image is from March 2009, while the second is from May 2011. The region was hit by a tsunami in March 2011, which caused drastic modifications to the landscape. The dataset contains 46836 pixels of change (~29.27%) and 113164 pixels of unchanged (~70.73%), the reference map being labeled by experts using a photointerpretation method.



Fig. 10. Fukushima TerraSAR-X image sequence. (a) March 2009. (b) May 2011.

C2) Results of the C²SOM Supervised Change Detection Model for Fukushima Dataset

Similar to the Mexico dataset, we have used a selection of 2000 pixels (1.25% of the total) for the training set, 552 labeled as change (~27.6% of the training set) and 1448 labels as no-change (~72.4% of the training set). The rest of 158000 pixels (98.75%) are used for testing.

Tables IX-XII and Figs. 11-13 show the results obtained by applying the C²SOM supervised model on the Fukushima SAR dataset. The results confirm the advantage of the CSOM classifier for change detection.

TABLE IX

BEST OVERALL ACCURACY (OA), AS A FUNCTION OF CLASSIFIER TYPE (SUPERVISED APPROACH-FUKUSHIMA DATASET).

Classifier	Parameters	False alarms		Missed alarms		Overall error	OA (%)	Kappa accuracy
		# pixels	%	# pixels	%			
1-NN	-	15269	13.68	18639	40.27	15269	78.53	0.471
Bayes	-	28071	25.15	8331	18	28071	76.94	0.506
MLP	1 hidden layer 9 neurons	8516	7.63	13751	29.71	8516	85.9	0.648
RBF	Spread=100	8550	7.66	14126	30.52	8550	85.64	0.641
SVM-RBF	spread=0.001	8603	7.7	13900	30.03	22503	85.76	0.639
CSOM	Rect sheet 5x7/3x7	7981	7.15	8470	18.3	7981	89.58	0.748

TABLE X

BEST MISS ALARM RATE (MAR) AS A FUNCTION OF CLASSIFIER TYPE (SUPERVISED APPROACH-FUKUSHIMA DATASET).

Classifier	Parameters	False alarms		Missed alarms		Overall error	OA (%)	Kappa accuracy
		# pixels	%	# pixels	%			
1-NN	-	15269	13.68	18639	40.27	33908	78.53	0.471
Bayes	-	28071	25.15	8331	18	36402	76.94	0.506
MLP	1 hidden layer 10 neurons	11709	10.49	11423	24.68	23132	85.35	0.647
RBF	Spread=64	10079	9.03	13316	28.77	23395	85.18	0.635
SVM-RBF	Spread = 0.004	8945	8.01	13595	29.37	22540	85.73	0.640
CSOM	Rect Sheet 5x8/10x10	28462	25.5	2647	5.72	31109	80.3	0.591

TABLE XI

BEST TOTAL OVERALL ACCURACY (OA) AS A FUNCTION OF CSOM ARCHITECTURE (MAR<25%) (SUPERVISED APPROACH-FUKUSHIMA DATASET).

Topology	SOM1/SOM2	False alarms		Missed alarms		Overall error	OA (%)	Kappa accuracy
		# pixels	%	# pixels	%			
Rect Toroid	6x5/4x6	9175	8.22	7628	16.48	16803	89.36	0.746
Rect Sheet	5x7/3x7	7981	7.15	8470	18.3	16451	89.58	0.748
Rect Cylinder	7x5/4x7	8818	7.90	8512	18.39	17330	89.02	0.736
Hex Toroid	7x5/5x5	8829	7.91	8401	18.15	17230	89.09	0.737
Hex Sheet	5x6/4x5	8126	7.28	8493	18.35	16619	89.48	0.745
Hex Cylinder	8x5/4x5	7813	7.00	9650	20.85	17463	88.94	0.730

TABLE XII

BEST MISS ALARM RATE (MAR) AS A FUNCTION OF CSOM ARCHITECTURE (OA>80%) (SUPERVISED APPROACH-FUKUSHIMA DATASET).

Topology	SOM1/SOM2	False alarms		Missed alarms		Overall error	OA (%)	Kappa accuracy
		# pixels	%	# pixels	%			
Rect Toroid	5x5/6x8	26486	23.73	3818	8.25	30304	80.80	0.595
Rect Sheet	5x8/10x10	28462	25.5	2647	5.72	31109	80.30	0.591
Rect Cylinder	5x12/10x14	27357	24.51	2995	6.47	30352	80.78	0.598
Hex Toroid	5x5/6x8	24377	21.84	3606	7.79	27983	82.27	0.622
Hex Sheet	5x5/9x7	28618	25.64	2754	5.95	31372	80.13	0.588
Hex Cylinder	5x8/10x11	25649	22.98	3101	6.7	28750	81.79	0.616

From Tables IX and X one can deduce that CSOM classifier maximizes Overall Accuracy (89.58%) and Kappa accuracy (0.748) for a rectangular sheet topology of module sizes 5x7/3x7. From Tables X and XII one can remark that CSOM also minimizes Miss alarm rate (5.72%), for CSOM modules of rectangular sheet with sizes 5x8/10x10.

Figs. 11 and 12 display the evolution of the OA and MAR indicators for square SOM modules, in the size range from 5x5 to 20x20 neurons.

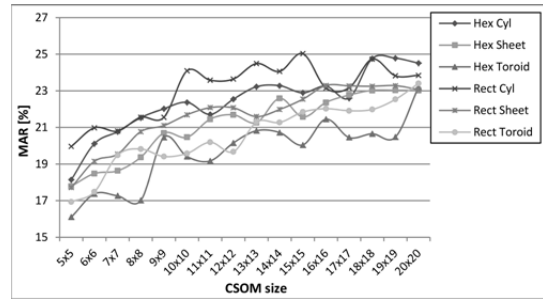


Fig. 11. Miss Alarm Rate (MAR) for different CSOM architectures as a function of SOM module size (Supervised approach-Fukushima dataset) (lower is better)

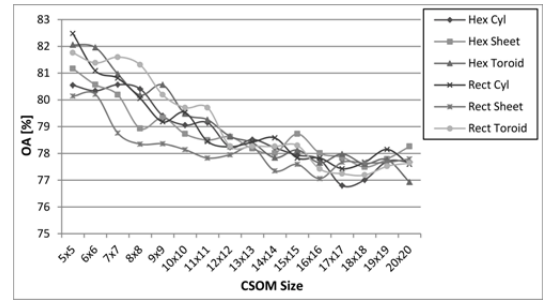


Fig. 12. Overall Accuracy (OA) for different CSOM architectures (Supervised approach-Fukushima dataset)

Fig. 13 shows the change detection map obtained by using the CSOM classifier that resulted in the best overall/kappa accuracy.

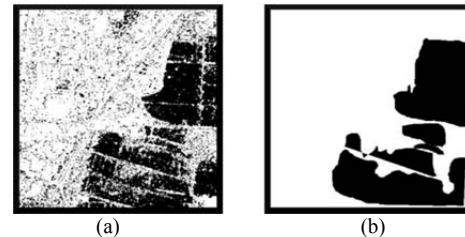


Fig. 13. (a) Change detection map obtained by the supervised approach with Fukushima dataset using CSOM (rectangular sheet with 5x7/3x7 size). (b) Reference change detection map (black pixels are changed; white pixels are unchanged).

C3) Results of the IC-USPS –C²SOM Unsupervised Change Detection Model for Fukushima SAR Dataset

As a result of unsupervised selection of the pseudo-training set (USP), one obtains 42281 changed pixels, 93719 unchanged pixels, and 24 000 unlabeled pixels. The test set contains all the image pixels, visually labeled to generate a kind of reference map.

The experimental results of the proposed unsupervised approach are given in Tables XIII-XVI. The change map obtained by the best classifier (CSOM with symmetrical hexa sheet modules of 6 x 18 neurons) is shown in Fig. 14.

TABLE XIII

BEST OVERALL ACCURACY (OA) AS A FUNCTION OF CLASSIFIER TYPE (UNSUPERVISED APPROACH-FUKUSHIMA DATASET).

Classifier	Parameters	False alarms		Missed alarms		Overall error	OA (%)	Kappa accuracy
		# pixels	%	# pixels	%			
1-NN	-	13683	12.09	12121	25.87	25804	83.87	0.614
Bayes	-	14601	12.90	11654	24.88	26255	83.59	0.610
MLP	1 hidden layer 15 neurons	14559	12.86	11686	24.95	26245	83.59	0.610
RBF	Spread = 200	13095	11.57	13202	28.18	26297	83.56	0.602
SVM-RBF	Spread = 0.001	12449	11.00	13203	28.18	25652	83.96	0.611
CSOM	Hex sheet 6x16/6x16	14555	12.86	10736	22.92	25291	84.19	0.627

TABLE XIV
BEST MISSED ALARM RATE (MAR) AS A FUNCTION OF CLASSIFIER TYPE
(UNSUPERVISED APPROACH-FUKUSHIMA DATASET).

Classifier	Parameters	False alarms		Missed alarms		Overall error	OA (%)	Kappa accuracy
		# pixels	%	# pixels	%			
1-NN	-	13683	12.09	12121	25.87	25804	83.87	0.614
Bayes	-	14601	12.90	11654	24.88	26255	83.59	0.610
MLP	1 hidden layer 10 neurons	14601	12.90	11654	24.88	26255	83.59	0.610
RBF	Spread = 300	21546	19.03	11724	25.03	33270	79.20	0.526
SVM-RBF	Spread = 10	14576	12.88	11670	24.91	26246	83.59	0.610
CSOM	Rect toroidal 6x12/6x12	20345	17.97	9399	20.06	29744	81.41	0.579

TABLE XV
BEST OVERALL ACCURACY (OA) AS A FUNCTION OF CSOM TOPOLOGY
(MAR<25%) (UNSUPERVISED APPROACH-FUKUSHIMA DATASET).

Topology	Symmetrical SOM module size	False alarms		Missed alarms		Overall error	OA (%)	Kappa accuracy
		# pixels	%	# pixels	%			
Rect. Sheet	6x14	14778	13.05	10679	22.80	25457	84.08	0.625
Hexa. Sheet	6x16	14555	12.86	10736	22.92	25291	84.19	0.627
Rect. Cylindrical	6x10	14926	13.18	10900	23.27	25826	83.85	0.619
Hexa. Cylindrical	6x14	15016	13.26	10702	22.84	25718	83.92	0.622
Rect. Toroidal	6x6	16567	14.63	10213	21.80	26780	83.26	0.611
Hexa. Toroidal	8x8	15750	13.91	10224	21.82	25974	83.76	0.621

TABLE XVI
BEST MISSED ALARM RATE (MAR) AS A FUNCTION OF CSOM TOPOLOGY
(OA>80%) (UNSUPERVISED APPROACH-FUKUSHIMA DATASET).

Topology	Symmetrical SOM module size	False alarms		Missed alarms		Overall error	OA (%)	Kappa accuracy
		# pixels	%	# pixels	%			
Rect. Sheet	4x4	17195	15.19	10081	21.52	27276	82.95	0.605
Hexa. Sheet	4x4	18363	16.22	9850	21.03	28213	82.36	0.595
Rect. Cylindrical	6x10	14926	13.18	10900	23.27	25826	83.85	0.619
Hexa. Cylindrical	6x18	16781	14.82	10170	21.71	26951	83.15	0.609
Rect. Toroidal	6x12	20345	17.97	9399	20.06	29744	81.41	0.579
Hexa. Toroidal	6x6	16965	14.99	10025	21.40	26990	83.13	0.609

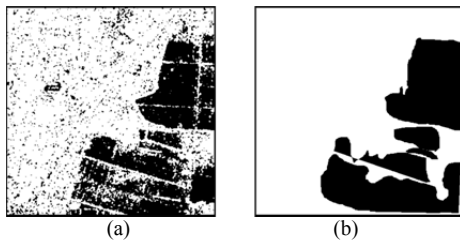


Fig. 14. (a) Change-detection map obtained by the unsupervised approach with the Fukushima dataset by using CSOM (hexagonal sheet symmetrical modules of 6x16 neurons). (b) Reference map. (black pixels are changed; white pixels are unchanged).

From Tables XIII - XVI one can deduce that CSOM leads to best performances by comparison to the considered benchmark classifiers. The best overall accuracy result of 84.19% and the best Kappa accuracy of 0.627 have been obtained for CSOM classifier (Table XIII). The best missed alarm rate of 20.06% (Table XIV) corresponds also to the CSOM classifier. Tables XV and XVI give the best performances (OA and respectively MAR) as a functions of CSOM module architecture and neighborhood lattice. The best OA is obtained using a CSOM architecture corresponding to a hexagonal sheet topology with symmetrical modules of size 6x16. The minimum MAR is obtained using a rectangular-toroidal architecture with symmetrical modules of sizes 6x12.

V. CONCLUDING REMARKS

The paper addresses a problem of high interest with large applications in Geomonitoring, namely change detection in remote sensing multitemporal images. The novelty of the paper consists in extending the use of Concurrent Self-Organizing

Maps (CSOM) classifier to change detection. Two CSOM-based approaches have been proposed, one for supervised and one for unsupervised change detection. The methods have been validated on two datasets, first one being obtained by a passive sensor (TM of LANDSAT-5) and the second dataset being acquired by an active sensor (TSX-1 of TerraSAR-X).

Experimental results confirms the effectiveness of the CSOM-based supervised/unsupervised change detection methods when compared with standard MLP-NN, RBF-NN, and SVM in terms of overall accuracy, kappa accuracy and error rate.

As future work direction, we prepare a fully neural model for unsupervised change detection, by substituting the Bayes-ME stage of the pseudo-training set selection with a neural technique.

REFERENCES

- [1] L. Bruzzone and D. F. Prieto, "Automatic analysis of the difference image for unsupervised change detection," *IEEE Trans. Geoscience and Remote Sensing*, vol. 38, no. 3, pp. 1171-1182, May 2000.
- [2] R. Amelard, A. Wong and D. A. Clausi, "Unsupervised classification of agricultural land cover using polarimetric synthetic aperture radar via a sparse texture dictionary model," in *Proc. Int'l Geoscience Remote Sensing Symp. (IGARSS 2013)*, Melbourne, July 2013.
- [3] D. Lu, P. Mausel, E. Brondizio and E. Moran, "Change detection techniques," *Int. J. Remote Sensing*, vol. 25, no. 12, pp. 2365-2401, 2004.
- [4] G. Mazzeo, F. Marchese, C. Filizzola, N. Pergola and V. Tramutoli, "A multi-temporal robust satellite technique (RST) for forest fire detection," in *Proc. Int. Workshop Analysis of Multi-Temporal Remote Sensing Images*, 2007.
- [5] L. Pulvirenti, M. Chini, F. Marzano, N. Pierdicca, S. Mori, L. Guerriero, G. Boni and L. Candela, "Detection of floods and heavy rain using cosmo-skymed data: the event in northwestern Italy of November 2011," in *Proc. Int'l Geoscience Remote Sensing Symp. (IGARSS 2012)*, Munich, 2012, pp. 3026-3029.
- [6] A. Singh, "Digital change detection techniques using remotely-sensed data," *Int. J. Remote Sensing*, vol. 10, no. 6, 1989.
- [7] M. V. N. Lima, CORINE Land Cover Updating for the year 2000: IMAGE 2000 and CLC 200, Products and Methods, European Environment Agency, J.R.C.
- [8] *** "CLC2006 Technical Guidelines," European Environment Agency, 2007.
- [9] F. Bovolo, C. Marin, L. Bruzzone, "A novel approach to building change detection in very high resolution SAR images," in *SPIE 2012, SPIE Conference on Image and Signal Processing for Remote Sensing XVIII*, Edinburgh, United Kingdom, 24-27 September 2012.
- [10] F. Bovolo and L. Bruzzone, "A split-based approach to unsupervised change detection in large-size multitemporal images: application to tsunami-damage assessment," *IEEE Trans. Geoscience and Remote Sensing*, vol. 45, no. 6, pp. 1658-1670, June 2007.
- [11] L. Bruzzone and F. Bovolo, "A Detail-Preserving Scale-Driven Approach to Unsupervised Change Detection in Multitemporal SAR Images," *IEEE Trans. Geoscience and Remote Sensing*, vol. 43, no. 12, pp. 2963-2972, 2005.
- [12] W. McGuire, B. McGuire, I. Mason and C. Kilburn, *Natural Hazards and Environmental Change: Key Issues in Environmental Change*, New York: Oxford Univ. Press, 2002.
- [13] F. Bovolo, L. Bruzzone and M. Marconcini, "A novel approach for unsupervised change detection based on semisupervised SVM and a similarity measure," *IEEE Trans. Geoscience and Remote Sensing*, vol. 46, no. 7, pp. 2070-2082, July 2008.
- [14] V. Neaogoe, R. Stoica and A. Ciurea, "A modular neural model for change detection in Earth Observation imagery," in *Proc. Int'l Geoscience Remote Sensing Symp. (IGARSS 2013)*, Melbourne, 2013, pp. 3321-3324.
- [15] F. Pacifici, F. del Frate, C. Solimini and W. Emery, "An innovative neural-net method to detect temporal changes in high resolution optical satellite imagery," in *IEEE Trans. Geoscience and Remote Sensing*, vol. 45, no 9, pp. 2940-2952, 2007.
- [16] A. Salberg and Ø.D. Trier, "Temporal analysis of multisensor data for forest change detection using hidden Markov models," in *Proc. Int'l Geoscience Remote Sensing Symp. (IGARSS 2012)*, Munich, 2012, pp. 6742-6752.
- [17] M. Volpi, D. Tuia, F. Bovolo, M. Kanevski and L. Bruzzone, "Supervised change detection in VHR images using contextual

information and support vector machines,” *Int. J. Applied Earth Observation and Geoinformation*, vol. 20, pp. 77-85, Feb. 2012.

- [18] F. Bovolo, S. Marchesi and L. Bruzzone, “A framework for automatic and unsupervised detection of multiple changes in multitemporal images,” *IEEE Trans. Geosci. Remote Sensing*, vol. 50, no. 6, pp. 2196-2212, June 2012.
- [19] R. Zurita-Milla, J. A. E. van Gijssel, N. A. S. Hamm, P. W. M. Augustijn and A. Vrieling, “Exploring spatiotemporal phenological patterns and trajectories using Self-Organizing Maps,” *IEEE Trans. Geoscience and Remote Sensing*, vol. 51, no. 4, pp. 1914-1921, Apr. 2013.
- [20] V. Neaogoe, M. Neghina and M. Datcu, “Neural network techniques for automated land-cover change detection in multispectral satellite time series imagery,” *Int. J. Mathematical Models and Methods In Applied Sciences*, vol. 6, no. 1, pp. 131-139, 2012.
- [21] T. Kohonen, “Self-Organizing Maps,” *Springer Series in Information Sciences*, 1995.
- [22] V. Neaogoe and A. Ropot, “Concurrent Self-Organizing Maps for pattern classification,” in *Proc. of First IEEE International Conference on Cognitive Informatics (ICCI 2002)*, Calgary, Aug. 2002, pp. 304-312.
- [23] V. Neaogoe and G. Strugaru, “A concurrent neural network model for pattern recognition in multispectral satellite imagery”, in *Proc. of the World Automation Congress (WAC 2008)*, Hawaii, Sept.-Oct. 2008.
- [24] M. Bishop, *Pattern Recognition and Machine Learning*, New York: Springer, 2006.



Victor-Emil Neaogoe (M’78–SM’84) received the M.S. degree in electronics and telecommunications engineering (Honor Diploma, ranking first place in his series of 300 graduates) and the Ph.D. degree in the same field from the Polytechnic Institute of Bucharest, Romania, in 1970 and 1976, respectively; he also received the M.S. degree in Applied Mathematics and Informatics from the University of Bucharest, Romania, in 1981. Since 1991 he has been a (Full) Professor at the “Politehnica” University of Bucharest, Romania,

where he teaches the following courses: pattern recognition and artificial intelligence; computational intelligence; data mining; detection, estimation and information processing. Prof. Neaogoe is the head of the Signal Processing, Pattern Recognition, Intelligent Systems and Data Mining Laboratory in the Department of Applied Electronics and Information Engineering, “Politehnica” University of Bucharest. He has been a Ph.D. supervisor since 1990. His current research interests are in the areas of pattern recognition, nature inspired intelligent techniques, Earth Observation image analysis, and sampling theory. Prof. Neaogoe is the author (or coauthor, in most cases as a first author) of about 150 papers published in referred international journals or conference proceedings. He has been invited as a plenary speaker in 10 international conferences and workshops and he has served on the Scientific Committee of many international conferences. Prof. Neaogoe has been included in Who’s Who in the World 2011, 2012, 2013, and 2014 (28th, 29th, 30th, and 31th Editions) as well as in Who’s Who in Science and Engineering 2011-2012 (11th Edition).



Radu-Mihai Stoica received the M.S. degree in Electronics, Telecommunications, and Information Technology and the Ph.D. degree in the same field from the “Politehnica” University of Bucharest, Romania, in 2008 and 2013, respectively. Radu has recently defended his Ph.D thesis titled “Artificial Intelligence Techniques for Pattern Recognition in Satellite Imagery”. His research interests focuses on multispectral satellite image analysis and pattern recognition.



Alexandru-Ioan Ciurea received the B.S., M.S., and Ph.D. degrees in Electronics, Telecommunications and Information Technology from “Politehnica” University of Bucharest in 2009, 2011, and 2014, respectively. In 2013 he has been for a 5 month Ph.D. stage at the Remote Sensing Laboratory in the Department of Information Engineering and Computer Science, University of Trento. Alexandru has recently presented his Ph.D. thesis titled “Advanced Pattern Recognition Techniques in Earth Observation Satellite Images”. His current research interests are related to pattern recognition in remote sensing imagery, change detection and telecommunications systems.



Lorenzo Bruzzone (S’95–M’98–SM’03–F’10) received the Laurea (M.S.) degree in electronic engineering (*summa cum laude*) and the Ph.D. degree in telecommunications from the University of Genoa, Italy, in 1993 and 1998, respectively. He is currently a Full Professor of telecommunications at the University of Trento, Italy, where he teaches remote sensing, radar, pattern recognition, and electrical communications. Dr. Bruzzone is the founder and the director of the Remote Sensing Laboratory in the Department of Information

Engineering and Computer Science, University of Trento. His current research interests are in the areas of remote sensing, radar and SAR, signal processing, and pattern recognition. He promotes and supervises research on these topics within the frameworks of many national and international projects. Among the others, he is the Principal Investigator of the *Radar for icy Moon exploration (RIME)* instrument in the framework of the *Jupiter ICy moons Explorer (JUICE)* mission of the European Space Agency. He is the author (or coauthor) of 150 scientific publications in referred international journals (101 in IEEE journals), more than 215 papers in conference proceedings, and 16 book chapters. He is editor/co-editor of 11 books/conference proceedings and 1 scientific book. His papers are highly cited, as proven form the total number of citations (more than 9850) and the value of the h-index (51) (source: Google Scholar). He was invited as keynote speaker in 24 international conferences and workshops. Since 2009 he is a member of the Administrative Committee of the IEEE Geoscience and Remote Sensing Society. Dr. Bruzzone ranked first place in the Student Prize Paper Competition of the 1998 IEEE International Geoscience and Remote Sensing Symposium (Seattle, July 1998). Since that time he was recipient of many international and national honors and awards. Dr. Bruzzone was a Guest Co-Editor of different Special Issues of international journals. He is the co-founder of the IEEE International Workshop on the Analysis of Multi-Temporal Remote-Sensing Images (MultiTemp) series and is currently a member of the Permanent Steering Committee of this series of workshops. Since 2003 he has been the Chair of the SPIE Conference on Image and Signal Processing for Remote Sensing. Since 2013 he has been the founder Editor-in-Chief of the IEEE GEOSCIENCE AND REMOTE SENSING MAGAZINE. Currently he is an Associate Editor for the IEEE TRANSACTIONS ON GEOSCIENCE AND REMOTE SENSING and the CANADIAN JOURNAL OF REMOTE SENSING. Since 2012 he has been appointed *Distinguished Speaker* of the IEEE Geoscience and Remote Sensing Society.



Francesca Bovolo (S’05–M’07–SM’13) received the “Laurea” (B.S.), the “Laurea Specialistica” (M.S.) degrees in telecommunication engineering (*summa cum laude*) and the Ph.D. in Communication and Information Technologies from the University of Trento, Italy, in 2001, 2003 and 2006, respectively where she has been a research fellow until June 2013.

She is the founder and the head of the Remote Sensing for Digital Earth unit at Fondazione Bruno Kessler (FBK), Trento, Italy and a member of the Remote Sensing Laboratory (RSLab) in Trento.

Her main research activity is in the area of remote-sensing image processing. Her interests are related to multitemporal remote sensing image analysis and change detection in multispectral, hyperspectral and SAR images, and very high resolution images, in particular. She conducts research on these topics within the context of several national and international projects. She is a referee for several international journals.

Dr. Bovolo ranked first place in the Student Prize Paper Competition of the 2006 *IEEE International Geoscience and Remote Sensing Symposium* (Denver, August 2006). Since January 2011 she is an associate editor of the *IEEE Journal of Selected Topics in Applied Earth Observations and Remote Sensing*. She has been guest editor for the Special Issue on “Analysis of Multitemporal Remote Sensing Data” of the *IEEE Transactions on Geoscience and Remote Sensing*. She is the Technical Chair of the Sixth International Workshop on the Analysis of Multi-temporal Remote-Sensing Images (MultiTemp 2011). From 2006 to 2013, she has served on the Scientific Committee of the SPIE International Conference on “Signal and Image Processing for Remote Sensing”. Since 2014 she is co-chair of the same conference. Since 2012 she is a member of the international program committee of the conference on *Pattern Recognition Applications and Methods*. She has served on the Scientific Committee of the *IEEE Fourth and Fifth International Workshop on the Analysis of Multi-Temporal Remote Sensing Images (MultiTemp 2007 and 2009)* and of the *IEEE GOLD Remote Sensing Conference* in 2010, 2012, and 2014.